Clinical Neurophysiology 153 (2023) 152–165

Contents lists available at ScienceDirect

Clinical Neurophysiology

journal homepage: www.elsevier.com/locate/clinph

Interindividual differences in posterior fossa morphometry affect cerebellar tDCS-induced electric field strength

Roderick P.P.W.M. Maas [a,*], Jennifer Faber [b,c], ESMI MR Study Group [1] Bart P.C. van de Warrenburg [a], Dennis J.L.G. Schutter [d]

[a] Department of Neurology, Donders Institute for Brain, Cognition, and Behaviour, Radboud University Medical Center, Nijmegen, the Netherlands
[b] German Center for Neurodegenerative Diseases (DZNE), Bonn, Germany
[c] Department of Neurology, University Hospital Bonn, Bonn, Germany
[d] Experimental Psychology, Helmholtz Institute, Utrecht University, Utrecht, the Netherlands

HIGHLIGHTS

- Skin-cerebellum distance is the dominant factor determining cerebellar tDCS-induced electric field strength in healthy adults.
- Interindividual differences in posterior fossa morphometry add unique explanatory variance to skin-cerebellum distance.
- When targeting the midline cerebellum, field strength and focality differ between cephalic and extracephalic electrode montages.

ARTICLE INFO

Article history:
Accepted 16 June 2023
Available online 14 July 2023

Keywords:
Cerebellar tDCS
Electric fields
Electrode position
Focality
Modelling study
Simulation

ABSTRACT

Objective: Clinical, behavioural, and neurophysiological effects of cerebellar transcranial direct current stimulation (tDCS) are highly variable and difficult to predict. We aimed to examine associations between cerebellar tDCS-induced electric field strength, morphometric posterior fossa parameters, and skin-cerebellum distance. As a secondary objective, field characteristics were compared between cephalic and extracephalic electrode configurations.

Methods: Electric field simulations of midline cerebellar tDCS (7 × 5 cm electrodes, current intensities of 2 mA) were performed on MRI-based head models from 37 healthy adults using buccinator, frontopolar, and lower neck reference electrodes. Average field strengths were determined in eight regions of interest (ROIs) covering the anterior and posterior vermis and cerebellar hemispheres. Besides skin-cerebellum distance, various angles were measured between posterior fossa structures. Multivariable linear regression models were used to identify predictors of field strength in different ROIs.

Results: Skin-cerebellum distance and "pons angle" were independently associated with field strength in the anterior and posterior vermis. "Cerebellar angle" and skin-cerebellum distance affected field strength in anterior and posterior regions of the right cerebellar hemisphere. Field strengths in all examined cerebellar areas were highest in the frontopolar and lowest in the lower neck montage, while the opposite was found for field focality. The lower neck montage induced considerably less spreading toward anterior cerebellar regions compared with the buccinator and frontopolar montages, which resulted in a more evenly distributed field within the cerebellum.

Conclusion: In addition to skin-cerebellum distance, interindividual differences in posterior fossa morphometry, specifically pons and cerebellar angle, explain part of the variability in cerebellar tDCS-induced electric field strength. Furthermore, when targeting the midline cerebellum with tDCS, an extracephalic reference electrode is associated with lower field strengths and higher field focality than cephalic montages.

* Corresponding author at: Department of Neurology, Donders Institute for Brain, Cognition, and Behaviour, Radboud University Medical Center, Geert Grooteplein Zuid 10, 6525 GA Nijmegen, the Netherlands.
E-mail address: roderick.maas@radboudumc.nl (R.P.P.W.M. Maas).
[1] ESMI MR Study Group: see the Appendix for a list of its members.

https://doi.org/10.1016/j.clinph.2023.06.019

Significance: This study identifies two novel subject-specific anatomical factors that partly determine cerebellar tDCS-induced electric field strength and reveals differences in field characteristics between electrode montages.

1. Introduction

Despite its modest size, the human cerebellum has been estimated to contain approximately 80% of neurons in the entire brain and to possess a surface area that is almost 80% of the neocortex (Azevedo et al., 2009; Sereno et al., 2020). The cerebellar cortex has reciprocal connections with essentially all supratentorial regions and is engaged in numerous networks subserving motor control, cognitive processing, and emotional regulation (Buckner et al., 2011; Krienen and Buckner, 2009). This functional diversity is reflected in the complex topographic manner by which the cerebellar cortex and its afferent and efferent projections are organized (Stoodley and Schmahmann, 2010). While the anterior lobe, lobule VIII, and medial parts of lobule VI contain face, arm, and leg representations, thereby comprising the sensorimotor cerebellum, lobules VI and VII are involved in various cognitive tasks and damage to these areas has been shown to induce cognitive impairments (Schmahmann, 2019). Moreover, the posterior vermis and fastigial nucleus have been extensively linked to emotional processing and are also known as the limbic cerebellum (Schmahmann, 2019; Stoodley and Schmahmann, 2010).

Modulation of cerebellar cortical activity with non-invasive brain stimulation techniques, such as transcranial direct current stimulation (tDCS), has not only enriched our understanding of the wide array of cerebellar functions, but is also considered a promising strategy to reduce motor, cognitive, and affective symptom severity in patients with neurological and psychiatric disorders (Benussi et al., 2023; Ferrucci et al., 2016; Grimaldi et al., 2016; Maas et al., 2020). Depending on the specific function, task, or symptom, one may select a unilateral hemisphere or midline montage. The latter seems particularly attractive when the vermis is the main target area, such as in studies of (pathologically disturbed) postural control, eye movements, and emotional processing (Cattaneo et al., 2022; Craig and Doumas, 2017; Ehsani et al., 2017; Ferrucci et al., 2012; Inukai et al., 2016; Panouilleres et al., 2015; Steiner et al., 2016). However, clinical and fundamental studies administering tDCS to the cerebellum often yield heterogeneous results, which is not only related to the positioning of electrodes and other stimulation-related parameters such as current intensity and session duration, but also to a considerable degree of between-subject variability in the susceptibility to tDCS (Fertonani and Miniussi, 2017; Li et al., 2015; Oldrati and Schutter, 2018; Polania et al., 2018). From a therapeutic point of view, interindividual differences may at least in part account for the overall null effects in several clinical trials and potentially limit the application of tDCS in patients with neurological and psychiatric diseases (Hulst et al., 2017; Maas et al., 2022b). Although various possible sources of interindividual variability in the response to cerebellar tDCS have been identified in recent years, further research into additional contributing factors is warranted to optimize and perhaps even personalize (treatment) protocols (Gomez-Tames et al., 2019; Klaus and Schutter, 2021; Li et al., 2015; Manto et al., 2022; Polania et al., 2018; Rezaee and Dutta, 2020).

Besides the physiological state and orientation of neurons in the target area relative to the current flow, accumulating evidence indicates an important role for local electric field strength in the neuromodulatory efficacy of tDCS (van Dun et al., 2016). Indeed, associations between individual field strengths and neurophysiological outcomes, including changes in motor evoked potential amplitudes, functional network connectivity, and gamma-aminobutyric acid (GABA) concentrations, have been reported with sensorimotor cortex stimulation (Antonenko et al., 2019; Laakso et al., 2019; Mosayebi-Samani et al., 2021; Nandi et al., 2022). A significant proportion of the variation in local field strength among healthy adults can be attributed to anatomical differences (Opitz et al., 2015).

Two initial modelling studies, based on one and three subjects, demonstrated the biophysical feasibility of reaching the cerebellum with tDCS applied over the lower occiput (Parazzini et al., 2014; Rampersad et al., 2014). In line with modelling research that focused on supratentorial areas, additional investigations with a larger number of head models have confirmed substantial interindividual variability in field strength and distribution within the cerebellum (Gomez-Tames et al., 2019; Klaus and Schutter, 2021; Rezaee and Dutta, 2020). Interestingly, skin-cerebellum distance emerged as the principal determinant, explaining more than half of the total variation in field strength underneath the target electrode (Gomez-Tames et al., 2019; Klaus and Schutter, 2021). It should be noted that a midline approach, aimed at targeting the vermis, has only been examined in one previous study, which exclusively used cephalic reference electrodes (Gomez-Tames et al., 2019). Direct comparisons between cephalic and extracephalic montages are currently lacking for cerebellar tDCS.

Driven by marked differences in posterior fossa morphometry between healthy adults, this study aimed to explore other subject-specific anatomical features that could explain additional variance in field strength following cerebellar tDCS. Furthermore, we evaluated possible differences in field characteristics between cephalic and extracephalic montages. Specifically, we (1) examined field strengths in eight regions of interest (ROIs) in the vermis and hemispheres of the anterior and posterior lobe using buccinator, frontopolar, and lower neck montages, (2) determined associations between field strength and morphometric posterior fossa parameters, and (3) applied multivariable linear regression models to identify factors that may independently predict field strength in different cerebellar regions.

2. Methods

2.1. Participants and study design

Thirty-seven adult volunteers (18 males; mean age 47.7 years [SD 12.7 years], range 22–69 years) who served as healthy controls in the prospective European Spinocerebellar ataxia type 3 / Machado-Joseph disease Initiative (ESMI) cohort study were included. None of them had a history of neurological or psychiatric disorders and Scale for the Assessment and Rating of Ataxia (SARA) scores were all below the acknowledged cutoff of three points (Schmitz-Hubsch et al., 2006). ESMI participants were recruited at eleven European centers and, additionally, at two Northern American sites. MRI scans were performed in Bonn (n = 14), Minneapolis (n = 6), Nijmegen (n = 5), Essen (n = 4), Aachen (n = 3), Heidelberg (n = 3), and Baltimore (n = 2). The local ethics committees of the contributing centers approved the study protocol. All participants provided written informed consent.

2.2. MRI acquisition

MRI data in all centers were acquired using 3T Siemens scanners with body coil transmission and 32-channel receive phased-array head coils (Skyra in Bonn and Nijmegen; Prisma in Aachen, Minneapolis, and Baltimore; Biograph in Essen; Trio in Heidelberg). T1-MPRAGE (192 slices, matrix size = 256 × 256, voxel size = 1 mm^3, repetition time = 2500 ms, echo time = 4.37 ms, inversion time = 1100 ms) and T2-FLAIR sequences (192 slices, matrix size = 256 × 256, voxel size = 1 mm^3, repetition time = 5000 ms, echo time = 397 ms, inversion time = 1800 ms) were recorded in sagittal direction. All MRI scans were checked for possible congenital abnormalities of the posterior fossa that may affect field strength and morphometric parameters (see below).

2.3. Electric field simulations

The *headreco* pipeline in SimNIBS version 3.2.6 was used to create tetrahedral volume meshes from individual MRI scans (Saturnino et al., 2019). Positions of EEG electrodes according to the international 10–10 system were automatically calculated based on four fiducial points (Jurcak et al., 2007). A 4 mm thick rectangular target electrode (7 × 5 cm) was added to the midline of each head model such that its center was situated 2 cm below the inion (Iz). Reference electrodes with similar dimensions and thickness were placed over the right cheek (buccinator montage), the middle of the forehead over Fpz (frontopolar montage), and as low as possible in the neck (right lower neck montage). As MRI scans in ESMI selectively included the brain and cervical spine, the lower cervical position represents the best possible approximation of the more commonly used deltoid montage. Simulations on a single anatomical model suggest that field strengths and spatial distribution in the cerebellum are roughly similar when the reference electrode is placed in the right lower neck compared with a position on the right shoulder (Supplementary Fig. 1).

All simulations were performed with a current intensity of 2 mA. Standard conductivity values were applied for the different tissue types in the mesh: σ_{scalp} = 0.465 S/m, σ_{skull} = 0.01 S/m, $\sigma_{cerebrospinal\ fluid}$ = 1.654 S/m, $\sigma_{grey\ matter}$ = 0.276 S/m, $\sigma_{white\ matter}$ = 0.126 S/m, and $\sigma_{eye\ balls}$ = 0.50 S/m (Rezaee and Dutta, 2019; Wagner et al., 2004; Windhoff et al., 2013). The field focality of each montage was determined in every subject as the volume of grey matter with a field strength (in V/m) equal to or higher than 50% or 75% of the 99.9th percentile (Saturnino et al., 2019).

2.4. Regions of interest

Eight regions of interest were selected that cover the vermis and hemispheres of the anterior and posterior lobe (Fig. 1). These were located in the vermis of lobule V (ROI1; MNI coordinates: x = 0, y = −66, z = −9; involved in postural control), right lobule V (ROI2; MNI coordinates: x = 15, y = −55, z = −16; involved in right hand movements and a finger sequence task), left lobule V (ROI3; MNI coordinates: x = −18, y = −53, z = −19; involved in left hand movements and a finger sequence task), right Crus II (ROI4; MNI coordinates: x = 24, y = −83, z = −40; involved amongst others in word reading, verb generation, and theory of mind), left Crus II (ROI5; MNI coordinates: x = −23, y = −82, z = −39; involved amongst others in interval timing and theory of mind), the vermis of lobule VIIIA (ROI6; MNI coordinates: x = 0, y = −70, z = −40; involved amongst others in emotional processing, hand movements, and a finger sequence task), right lobule VIIIA (ROI7; MNI coordinates: x = 21, y = −61, z = −52; involved amongst others in right hand movements and a finger sequence task), and left lobule VIIIA (ROI8; MNI coordinates: x = −21, y = −59, z = −57; involved amongst others in left hand movements and a finger sequence task) (King et al., 2019). After transforming these coordinates from MNI to subject space with the mni2subject_coords function in SimNIBS, average field strengths were obtained in each ROI with a radius of 5 mm.

2.5. Morphometric posterior fossa parameters

Four different angles were evaluated on a midsagittal MRI slice in each individual (Fig. 2). First, the tentorial angle (T) was measured between a line through the tentorium and a line drawn from the nasion through the tuberculum sellae. We anticipated that a steeper tentorium, indicated by a larger tentorial angle, is associated with lower field strengths in the cerebellum, especially in the anterior areas. Second, the cerebellar angle (C) was defined by a line through the tentorium and a line from the opisthion to the most "curved" position of the posterior fossa cerebrospinal fluid (CSF) space directly behind the cerebellum. We reasoned that a smaller cerebellar angle would result in higher field strengths in the cerebellum. Third, the pons angle (P) was created by the intersection of a line through the dorsal surface of the pons and a line through the tentorium. We presumed that a larger pons angle would increase the "window" for the cerebellum, resulting in higher field strengths following cerebellar tDCS. Finally, the occipital angle (O) was formed by a line drawn from the nasion through the tuberculum sellae and a line from the opisthion through the most curved position of the posterior fossa CSF space directly behind the cerebellum. We hypothesized that a larger occipital angle would be associated with higher field strengths in the cerebellum.

2.6. Skin-cerebellum distance

After defining the position of the inion on a midsagittal MRI slice, the shortest (perpendicular) distance was measured between the skin approximately 2 cm below this point (i.e., the imaginary center of the target electrode) and the outer surface of the vermis in ITK-SNAP version 3.8.0 (Yushkevich et al., 2006). Similar measurements were performed for the left and right cerebellar hemisphere at points halfway between the vermis and the most lateral parts of the cerebellum.

2.7. Statistical analysis

Average field strengths in each ROI and field focality values were compared between the three montages using one-way repeated measures analysis of variance (ANOVA) followed by Bonferroni post hoc tests. The assumption of sphericity was checked with Mauchly's test and Greenhouse-Geisser corrections were applied if necessary.

To evaluate if within-subject field strengths were consistently associated across montages, Pearson correlation coefficients were determined. Associations between field strength and skin-cerebellum distance (midline measurement for ROIs 1 and 6; right-sided measurements for ROIs 2, 4, and 7; left-sided measurements for ROIs 3, 5, and 8), morphometric posterior fossa parameters, and age were assessed with Pearson correlation coefficients.

Stepwise multivariable linear regression was performed to identify factors that are independently associated with field strength. Based on the results of univariate analyses, skin-cerebellum distance, cerebellar angle, pons angle, and occipital angle were selected as predictor variables. In order to limit the number of regression analyses and comparisons, we (1) focused on the extracephalic montage, which was used in our own and other trials (Benussi et al., 2017; Maas et al., 2022a; Maas et al., 2022b), and (2) selected two ROIs in the anterior and posterior vermis and three ROIs within the right cerebellar hemisphere. Statis-

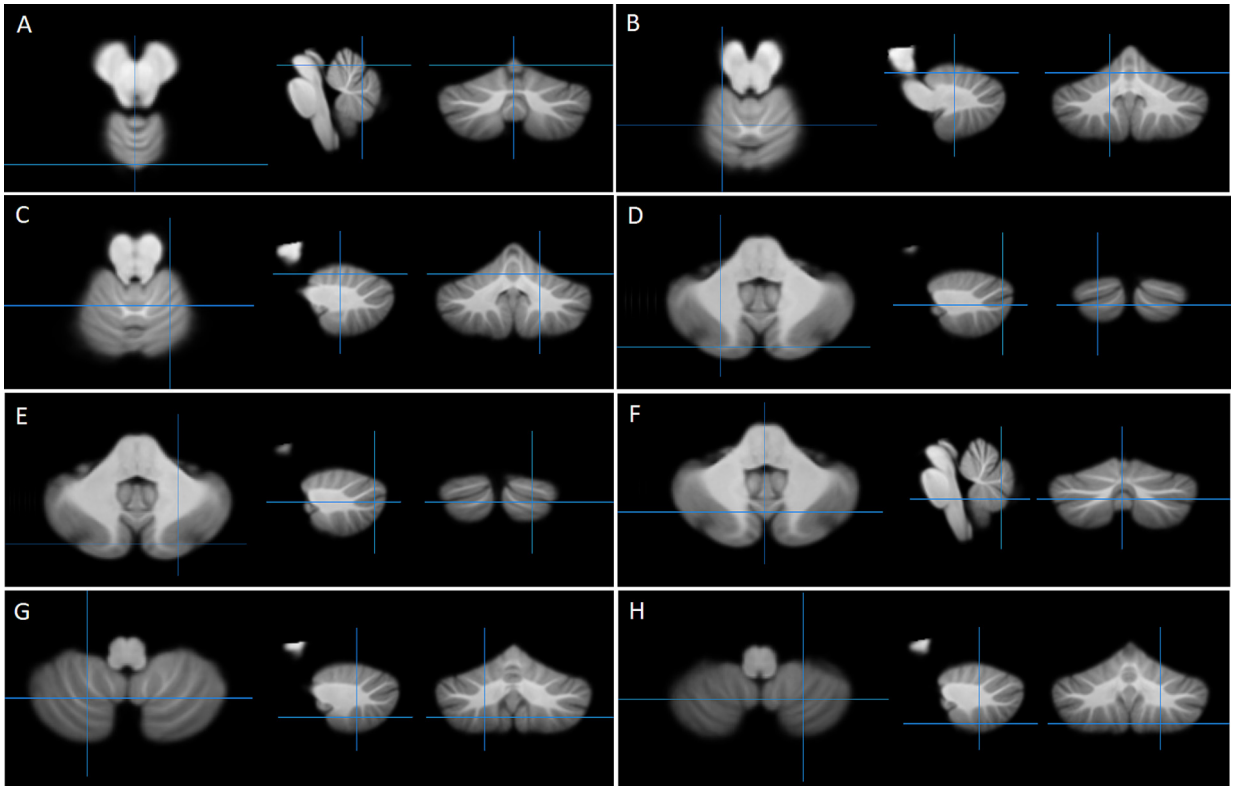

Fig. 1. Axial, sagittal, and coronal images demonstrating the centers of the eight selected regions of interest (ROIs). These include the vermis of lobule V (A, ROI1, MNI coordinates: x = 0, y = −66, z = −9), right lobule V (B, ROI2, MNI coordinates: x = 15, y = −55, z = −16), left lobule V (C, ROI3, MNI coordinates: x = −18, y = −53, z = −19), right Crus II (D, ROI4, MNI coordinates: x = 24, y = −83, z = −40), left Crus II (E, ROI5, MNI coordinates: x = −23, y = −82, z = −39), the vermis of lobule VIIIA (F, ROI6, MNI coordinates: x = 0, y = −70, z = −40), right lobule VIIIA (G, ROI7, MNI coordinates: x = 21, y = −61, z = −52), and left lobule VIIIA (H, ROI8, MNI coordinates: x = −21, y = −59, z = −57).

tical analyses were conducted in SPSS Statistics (IBM, version 27) and GraphPad Prism 9.3.1. The level of significance was set at 0.05 (two-tailed).

3. Results

One participant had a retrocerebellar arachnoid cyst and was excluded from the analyses of morphometric parameters.

3.1. Effects of electrode montage on electric field strength, distribution, and focality

As illustrated in Fig. 3, one-way repeated measures ANOVA revealed a significant effect of montage on average field strength in all examined cerebellar regions ($p < 0.001$ for all ROIs, eta squared range 0.81–0.98). Post hoc Bonferroni-corrected comparisons showed differences between the lower neck and buccinator montage ($p < 0.001$ for all ROIs, Cohen's d range 0.85–3.14), between the lower neck and frontopolar montage ($p < 0.001$ for all ROIs, Cohen's d range 1.50–4.79), and between the buccinator and frontopolar montage ($p < 0.001$ for all ROIs, Cohen's d range 0.43–2.08). Field strengths in the anterior and posterior vermis and in both cerebellar hemispheres were highest in the frontopolar and lowest in the lower neck montage. Irrespective of electrode placement, values were highest at the surface of right Crus II and lowest in left lobule V (for the lower neck and buccinator montage) or right lobule V (for the frontopolar montage).

The relative difference in average field strength between right Crus II and left or right lobule V was more pronounced in the lower neck montage than in the buccinator and frontopolar montages (52.6%, 30.9%, and 21.0% on the group level, respectively). These comparisons suggest that an extracephalic reference electrode induces less spreading toward anterior cerebellar areas, while cephalic electrode configurations may lead to more evenly distributed electric fields within the cerebellum (Fig. 4). Indeed, one-way repeated measures ANOVA confirms a significant effect of montage on field focality [F (1.72, 62.0) = 41.56, $p < 0.001$, eta squared = 0.54]. The average volume of grey matter with a field strength equal to or higher than 75% of the 99th percentile was 1.5 and 1.7 times lower in the lower neck montage (mean ± SD, 8.4 ± 2.5 cm^3) compared with the buccinator montage (mean ± SD, 12.8 ± 3.7 cm^3, $p < 0.001$, Cohen's d = 1.38) and frontopolar montage (mean ± SD, 14.1 ± 4.6 cm^3, $p < 0.001$, Cohen's d = 1.54), respectively, indicating higher focality with an extracephalic reference electrode (Fig. 5). When the threshold was lowered to 50% of the 99th percentile, differences between the lower neck montage (mean ± SD, 43.1 ± 12.6 cm^3), buccinator montage (mean ± SD, 117.2 ± 31.1 cm^3), and frontopolar montage (mean ± SD, 194.3 ± 57.7 cm^3) were much larger [F (1.22, 44.07) = 266.24, $p < 0.001$ overall as well as for all pairwise comparisons, eta squared = 0.88, Cohen's d range 1.66–3.62]. Replicating earlier findings, extracerebellar current spread was mainly observed in the right temporal lobe when the reference electrode was positioned over the right cheek (buccinator), while a more diffuse field with relatively high values in the prefrontal areas was found with a frontopolar montage (Klaus and Schutter, 2021).

As illustrated in Fig. 6, within-subject field strengths across montages were highly correlated in all ROIs (lower neck vs. buccinator: Pearson's r range 0.79–0.94, all p values < 0.001; lower neck vs. frontopolar: Pearson's r range 0.73–0.92, all p values < 0.001;

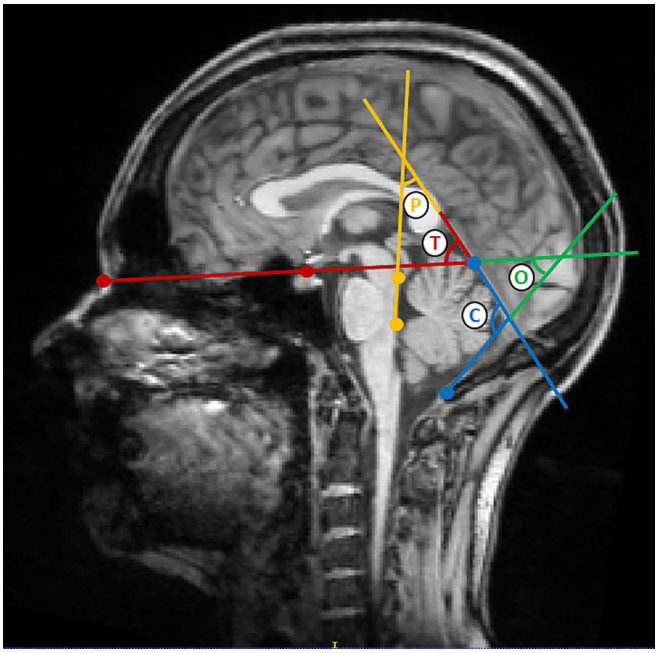

Fig. 2. Midsagittal MRI slice illustrating the pons angle (P), tentorial angle (T), occipital angle (O), and cerebellar angle (C). The pons angle was defined by a line through the dorsal surface of the pons and a line through the tentorium. The tentorial angle was measured between a line through the tentorium and a line drawn from the nasion through the tuberculum sellae. The occipital angle was created by the intersection of a line drawn from the nasion through the tuberculum sellae and a line from the opisthion through the most curved position of the posterior fossa CSF space directly behind the cerebellum. Finally, the cerebellar angle was formed by the latter line and a line through the tentorium.

buccinator vs. frontopolar: Pearson's r range 0.94–0.99, all p values < 0.001).

3.2. Effects of interindividual anatomical variability on electric field strength

Average field strengths in each of the ROIs were inversely associated with skin-cerebellum distance in all three montages (Pearson's r range −0.65 to −0.80, all p values < 0.001) (Fig. 7). Significant correlations were also found between field strength and occipital angle, cerebellar angle, and pons angle, which were most pronounced for the lower neck montage (occipital angle: Pearson's r range −0.34 to −0.48, p range 0.003 to 0.041; cerebellar angle: Pearson's r range −0.34 to −0.44, p range 0.007 to 0.041; pons angle: Pearson's r range 0.32 to 0.47, p range 0.004 to 0.055) (Fig. 8 and Supplementary Tables S1–S3). By contrast, tentorial angle was not related to field strength in any of the examined montages (Pearson's r range −0.18 to 0.06, p range 0.30 to 0.99). Finally, there were no significant associations between field strengths and age (Pearson's r range −0.30 to 0.01, p range 0.076 to 0.96).

3.3. Independent predictors of electric field strength

Stepwise multivariable linear regression analyses were performed to identify factors that might predict field strengths in a selection of ROIs with an extracephalic montage. Based on the results of the abovementioned univariate analyses, skin-cerebellum distance, cerebellar angle, pons angle, and occipital angle were chosen as independent variables. Unstandardized coefficients (b) and their 95% confidence intervals, standardized coefficients (beta), R^2 values, and improvements in R^2 are summarized in Table 1.

Average field strength in the anterior and posterior vermis was found to be independently affected by skin-cerebellum distance ($p < 0.001$ for both ROIs) and pons angle ($p = 0.014$ for ROI1 [lobule V]; $p = 0.005$ for ROI6 [lobule VIIIA]). Compared with a model that only contained skin-cerebellum distance, the addition of pons angle improved the R^2 value with 0.08 and 0.09 to 0.60 and 0.64, respectively. These findings indicate that pons angle explains 8–9% of the variance in field strength in the vermis.

Similar to both midline regions, skin-cerebellum distance was the most important factor associated with electric field strength in right lobule V (ROI2), Crus II (ROI4), and lobule VIIIA (ROI7). Moreover, the cerebellar angle was found to be a second independent predictor of field strength in these areas ($p = 0.002$ for ROI2; $p = 0.033$ for ROI4; $p = 0.002$ for ROI7), accounting for an additional 5% (Crus II), 10% (lobule V), and 11% (lobule VIIIA) of variance and resulting in R^2 values of 0.66–0.69.

4. Discussion

Inspired by the variability in clinical, behavioural, and neurophysiological outcomes across cerebellar tDCS studies, we used computational modelling to examine how strength and distribution of the induced electric field within the cerebellum are affected by interindividual differences in posterior fossa morphometry. Furthermore, we compared field characteristics between the buccinator, frontopolar, and lower neck montages. The main results of this study can be summarized as follows. First, replicating previous findings, our data confirm that skin-cerebellum distance is the dominant factor determining tDCS-induced field strength throughout the cerebellum. Second, pons angle was independently associated with field strengths in the anterior and posterior vermis, while cerebellar angle predicted field strengths in the right cerebellar hemisphere. Both morphometric posterior fossa parameters added unique explanatory variance to skin-cerebellum distance. Third, compared with the extracephalic lower neck montage, both cephalic configurations induced higher field strengths in all examined cerebellar regions. As grey matter volumes with field strengths equal to or higher than 50% or 75% of peak values were also significantly larger in the frontopolar and buccinator montage, the increased field strengths came at the expense of focality.

In agreement with previous modelling studies, skin-cerebellum distance was the strongest predictor of electric field strength in all ROIs, accounting for 50–60% of variance (Gomez-Tames et al., 2019; Klaus and Schutter, 2021). Here, we demonstrate that a systematic investigation of morphometric posterior fossa features, specifically pons and cerebellar angle, adds approximately 10%, indicating that anatomical factors together explain 60–70% of the interindividual variability in field strength when tDCS is applied over the midline. We hypothesize that a larger pons angle and a smaller cerebellar angle increase the volume of cerebellar cortex potentially amenable to the modulatory effects of cerebellar tDCS. In contrast to our hypothesis, steepness of the tentorium, as expressed by the tentorial angle, did not affect electric field strength in any of the selected ROIs, which suggests that this measure is less relevant for tDCS modelling studies in neurotypical subjects. Furthermore, although occipital angle correlated with electric field strength in several ROIs in univariate analyses, it was not retained in multivariable linear regression models. Finally, this study did not show significant associations between age and field strengths, which may be explained by the relatively small proportion of individuals aged 60 years or older (i.e., 16%). Indeed, cerebellar shrinkage in healthy elderly people has been reported to start between 50 and 60 years of age (Luft et al., 1999). Further

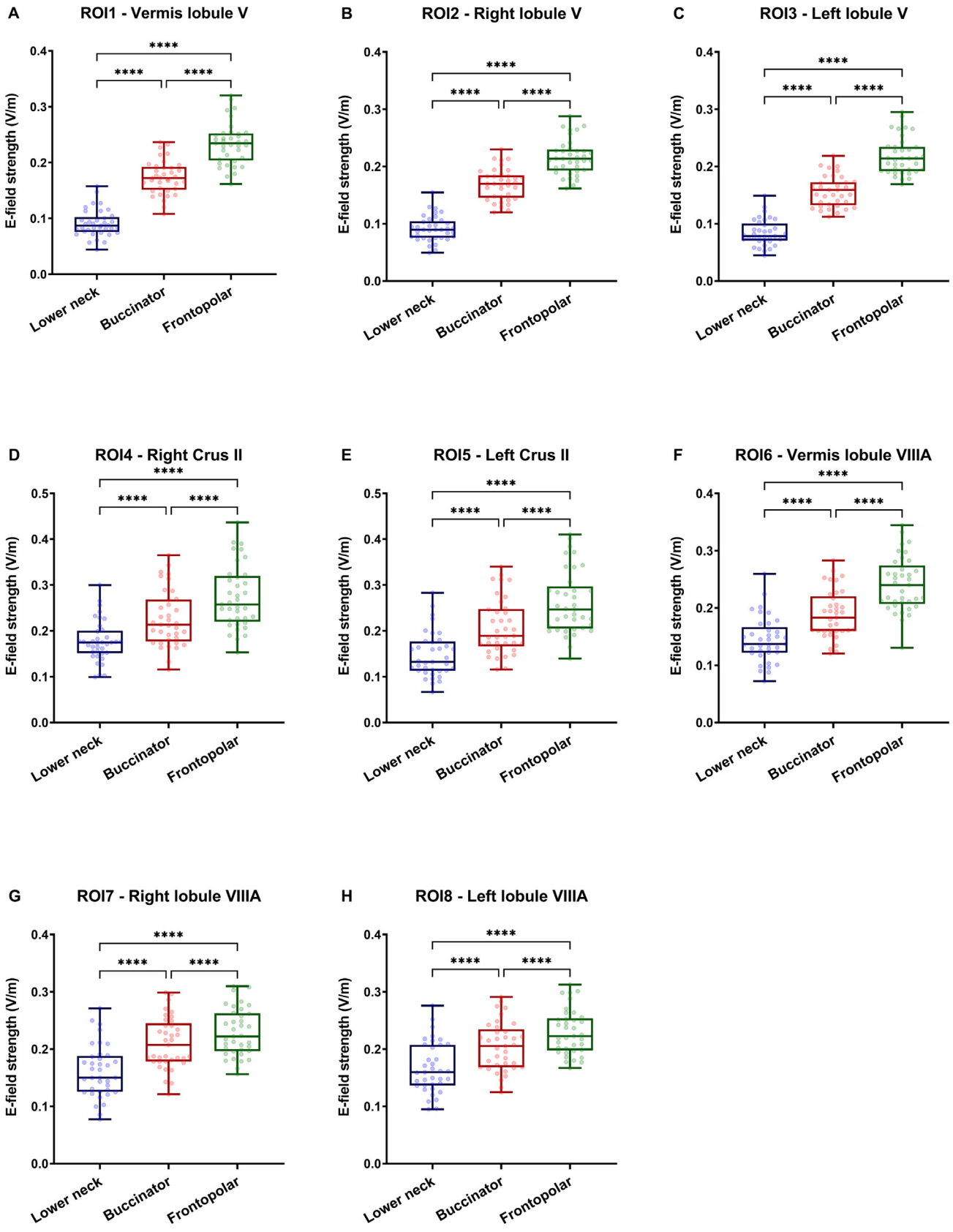

Fig. 3. Electric field strengths induced by cerebellar transcranial direct current stimulation in each of the eight selected regions of interest (ROIs) using different electrode configurations. Whiskers represent the minimum and maximum values. **** indicates a p value < 0.001.

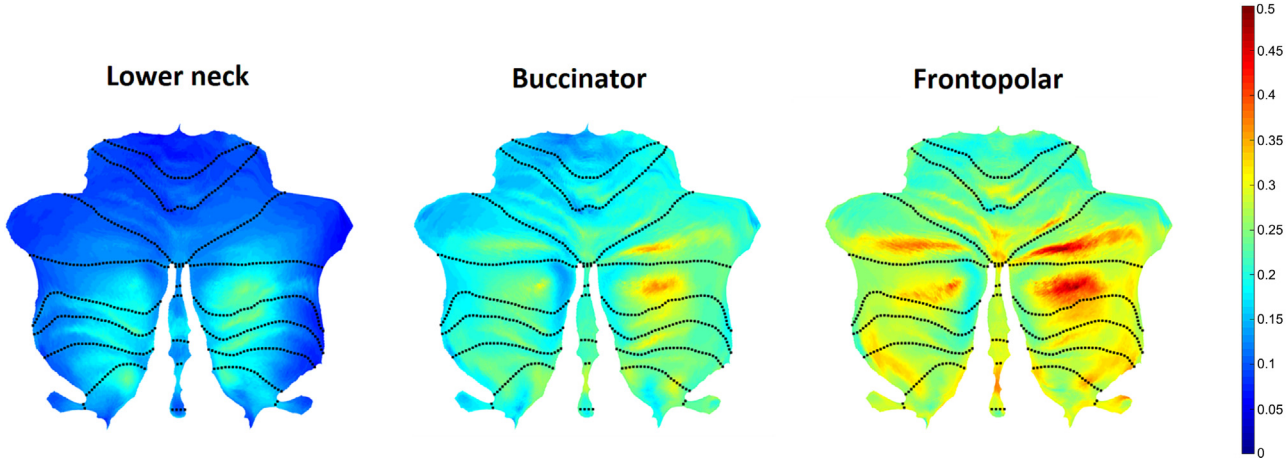

Fig. 4. Cerebellar flatmaps of a representative healthy individual illustrating the distribution of the electric field (in V/m) induced by cerebellar transcranial direct current stimulation with different montages.

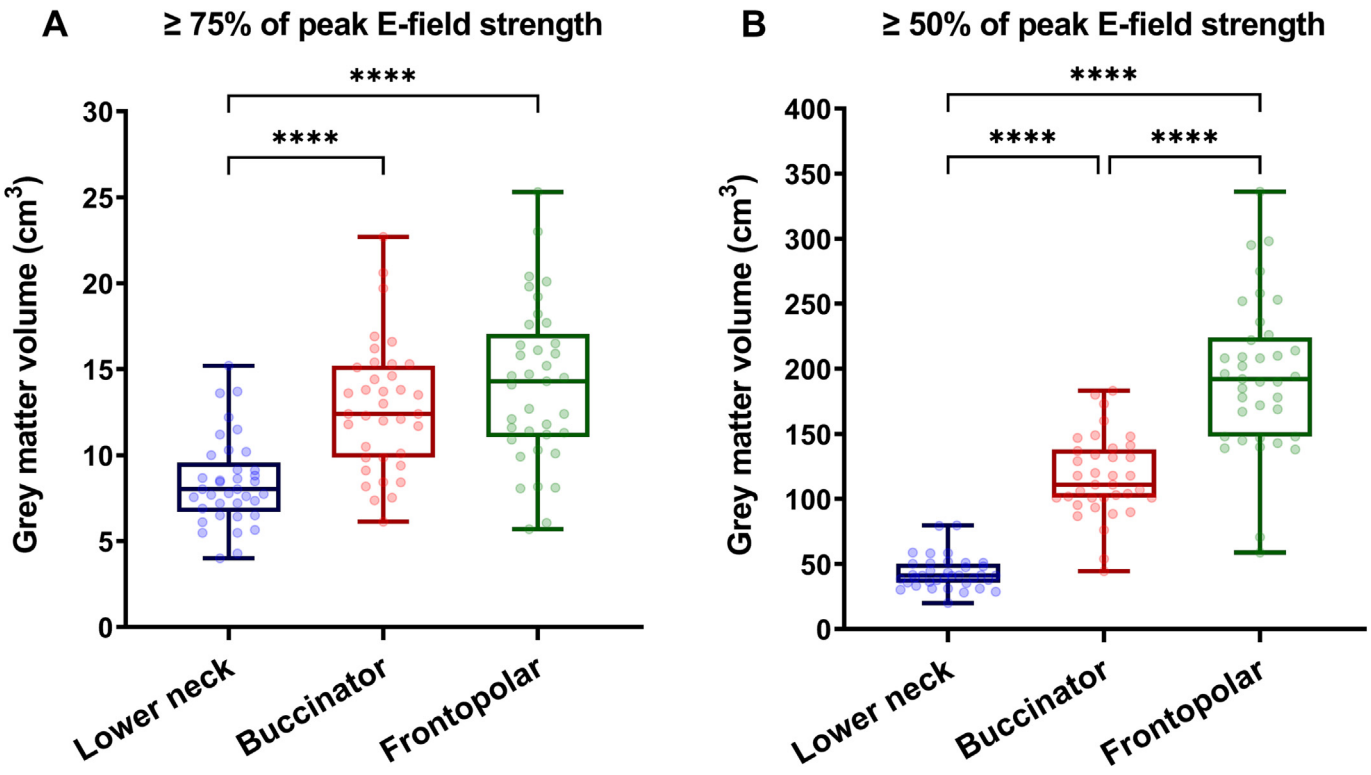

Fig. 5. Focality of the electric field induced by cerebellar transcranial direct current stimulation in different montages. Shown are the volumes of grey matter with a field strength equal to or higher than 75% (A) or 50% (B) of the 99.9th percentile. Whiskers represent the minimum and maximum values. **** indicates a p value < 0.001.

research is required to evaluate whether similar associations between posterior fossa parameters and tDCS-induced electric field strength can be found in patients with cerebellar and pontine atrophy due to degenerative diseases.

Reference electrodes in clinical and fundamental cerebellar tDCS research are most commonly placed on the forehead, cheek, or shoulder (van Dun et al., 2016). This is the first modelling study that compared differences in field strength between cephalic and extracephalic montages. Gomez-Tames and colleagues also performed electric field simulations of a midline approach (in addition to hemispherical approaches), but exclusively used cephalic reference electrodes. These investigators similarly found higher field strengths in the cerebellum with a frontopolar montage compared with a buccinator montage, but did not report statistical comparisons (Gomez-Tames et al., 2019). Furthermore, Klaus and Schutter (2021) recently described differences in field focality between a series of montages in which the target electrode was positioned over the right cerebellar hemisphere, with significantly higher focality when physical distance between electrodes decreased.

The main limitation of the present work is the absence of behavioural and neurophysiological correlates, such as motor learning paradigms, cerebellar brain inhibition, or blink reflex excitability. Besides electric field strength, several other sources of interindividual variability in tDCS effects have been identified, including genetic polymorphisms, age, differences in arousal or attentional

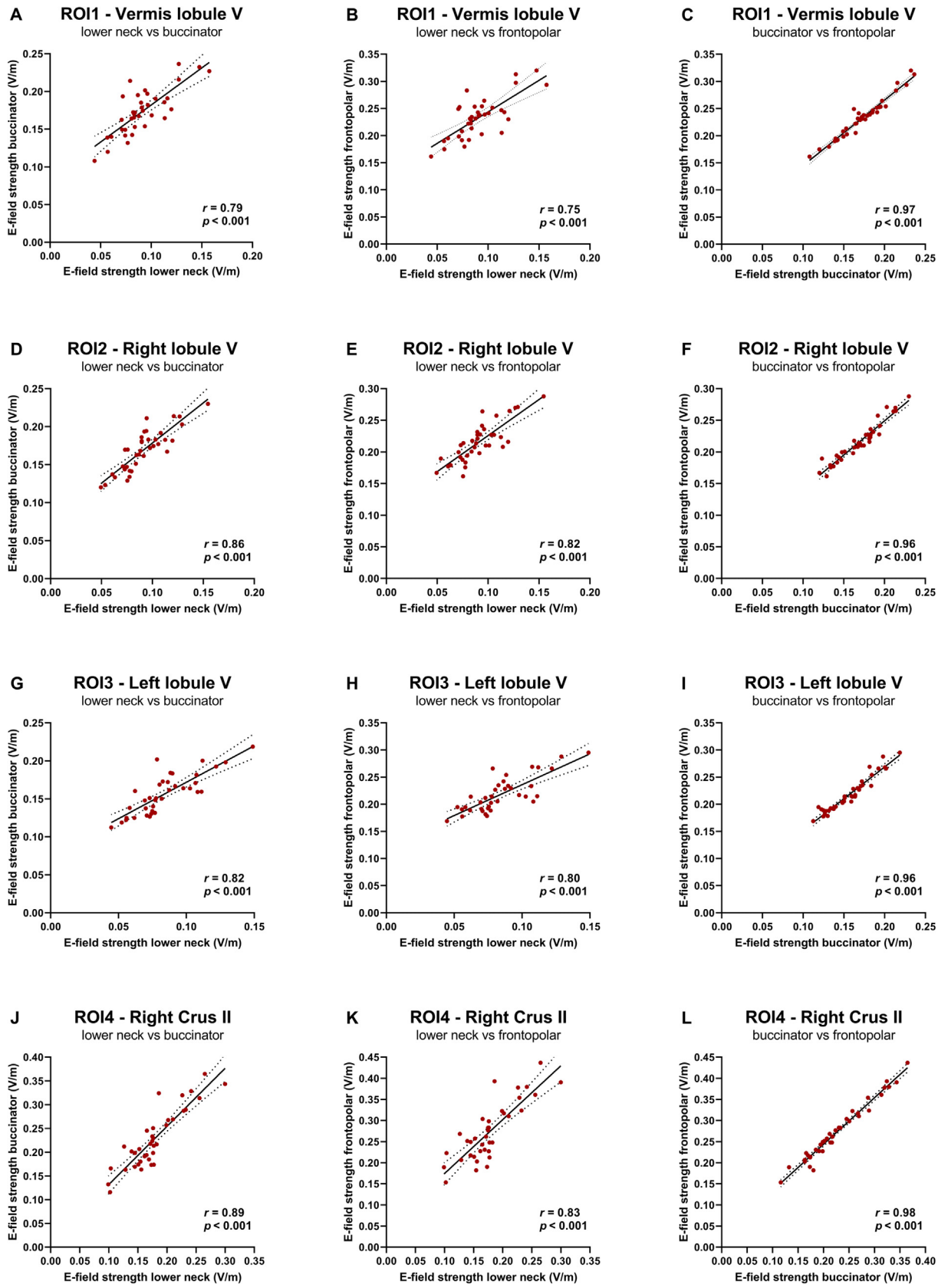

Fig. 6. Associations between electric field strengths in each of the eight selected regions of interest (ROIs) across different montages. Shown are the correlations between the lower neck and buccinator montages (A, D, G, J, M, P, S, and V), between the lower neck and frontopolar montages (B, E, H, K, N, Q, T, and W), and between the buccinator and frontopolar montages (C, F, I, L, O, R, U, and X).

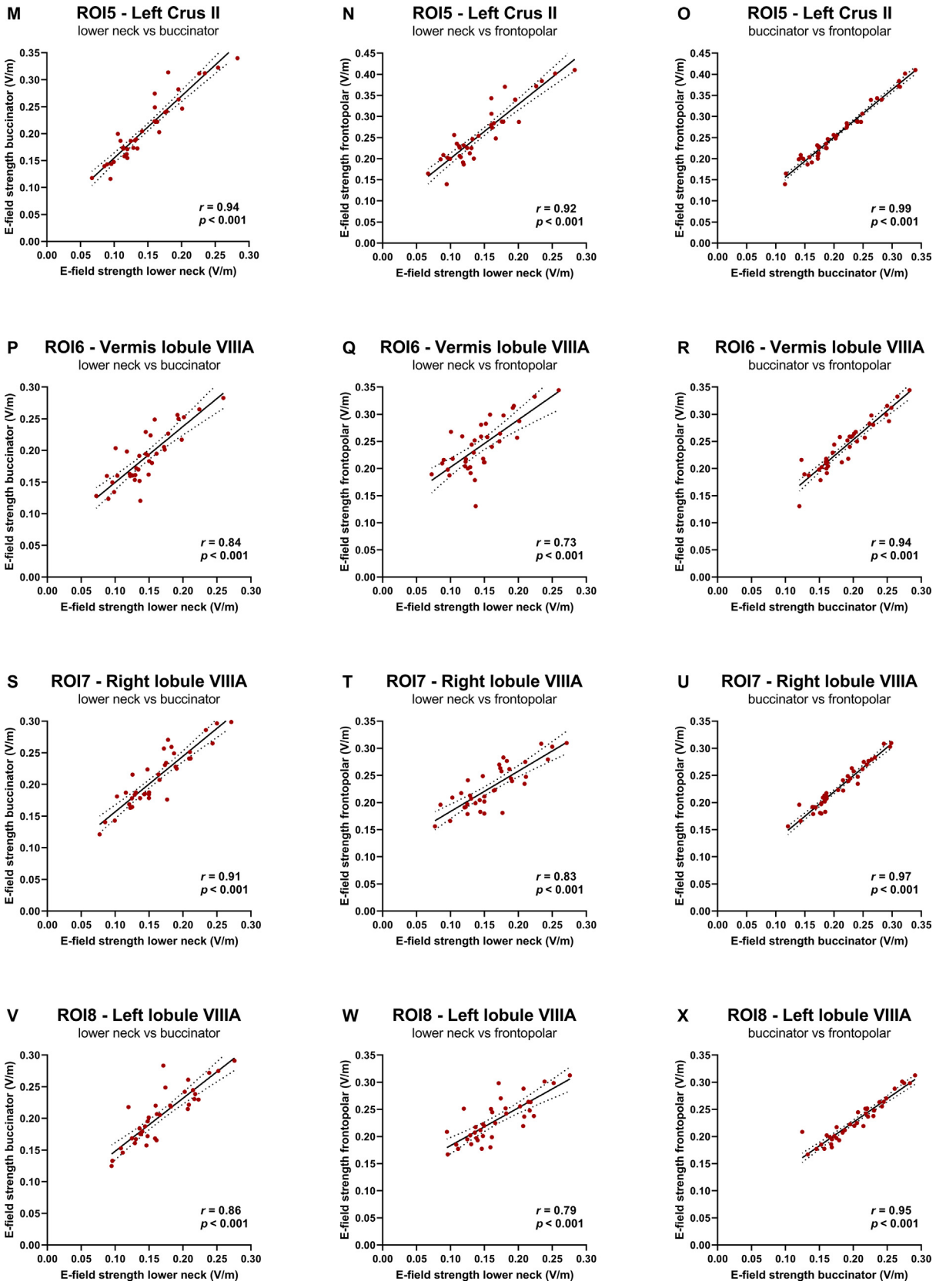

Fig. 6 (*continued*)

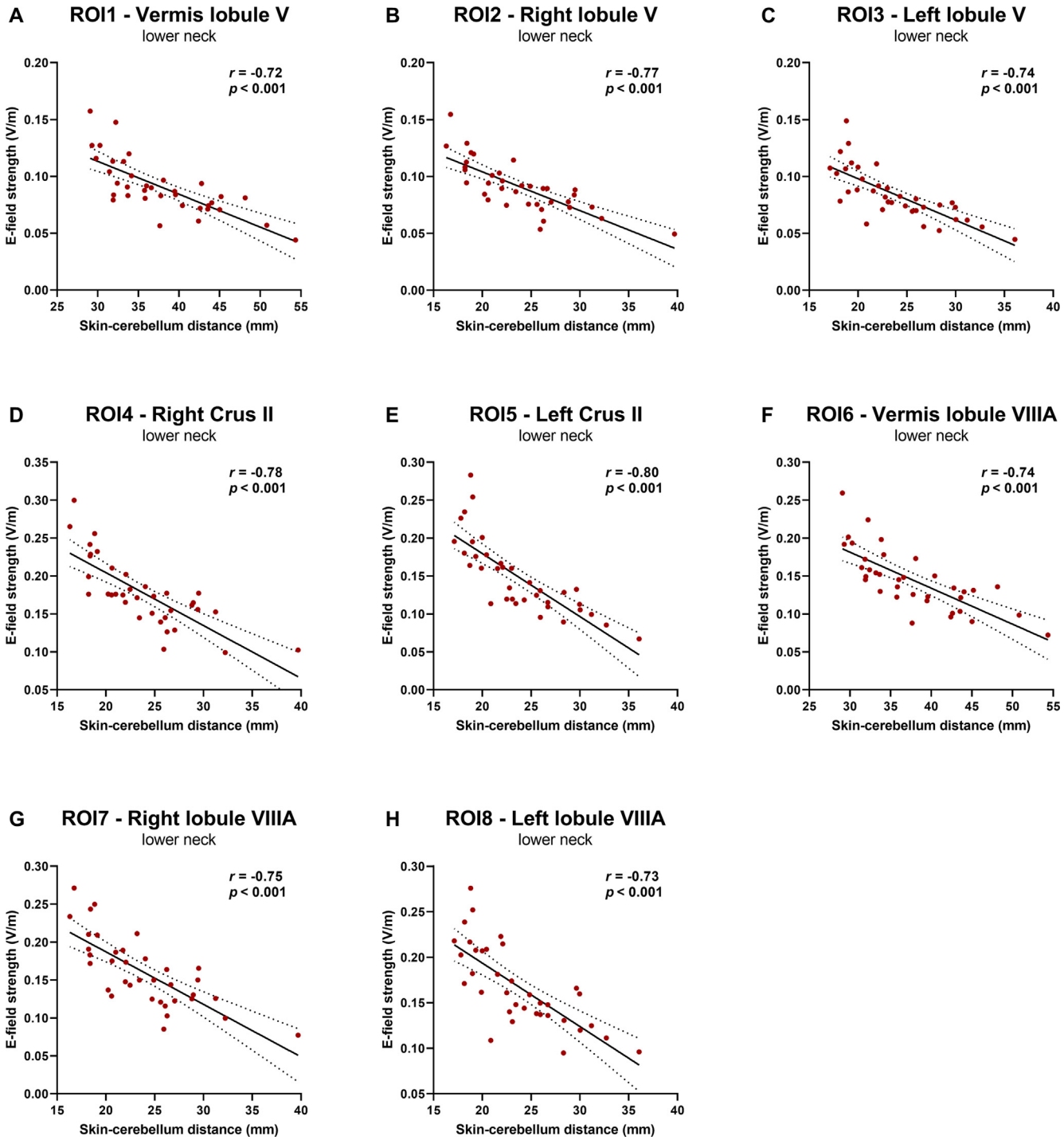

Fig. 7. Associations between electric field strength in each of the eight selected regions of interest (ROIs) and skin-cerebellum distance using a lower neck montage.

state, and the complex folding of the cerebellum (Li et al., 2015; Polania et al., 2018). It should be emphasized that our results mainly serve as a theoretical basis for future cerebellar tDCS studies, which may explore correlations between the predicted field strength in a target area and actually observed clinical, behavioural, or neurophysiological effects. Although such associations have yet to be established for less extensively investigated target regions, such as the cerebellum, emerging evidence from sensorimotor cortex tDCS suggests that neuromodulatory effects are related to absolute field strength values (Antonenko et al., 2019; Laakso et al., 2019; Mosayebi-Samani et al., 2021; Nandi et al., 2022).

In order to potentially reduce the variability of results following cerebellar tDCS, studies with small sample sizes may benefit from routinely performing brain MRI scans to measure skin-cerebellum distance and to evaluate morphometric posterior fossa features beforehand. Proper selection of participants could be an important step that might increase the likelihood of obtaining more consistent outcomes, especially in therapeutic trials. Furthermore, asymptomatic congenital abnormalities of the posterior fossa, such

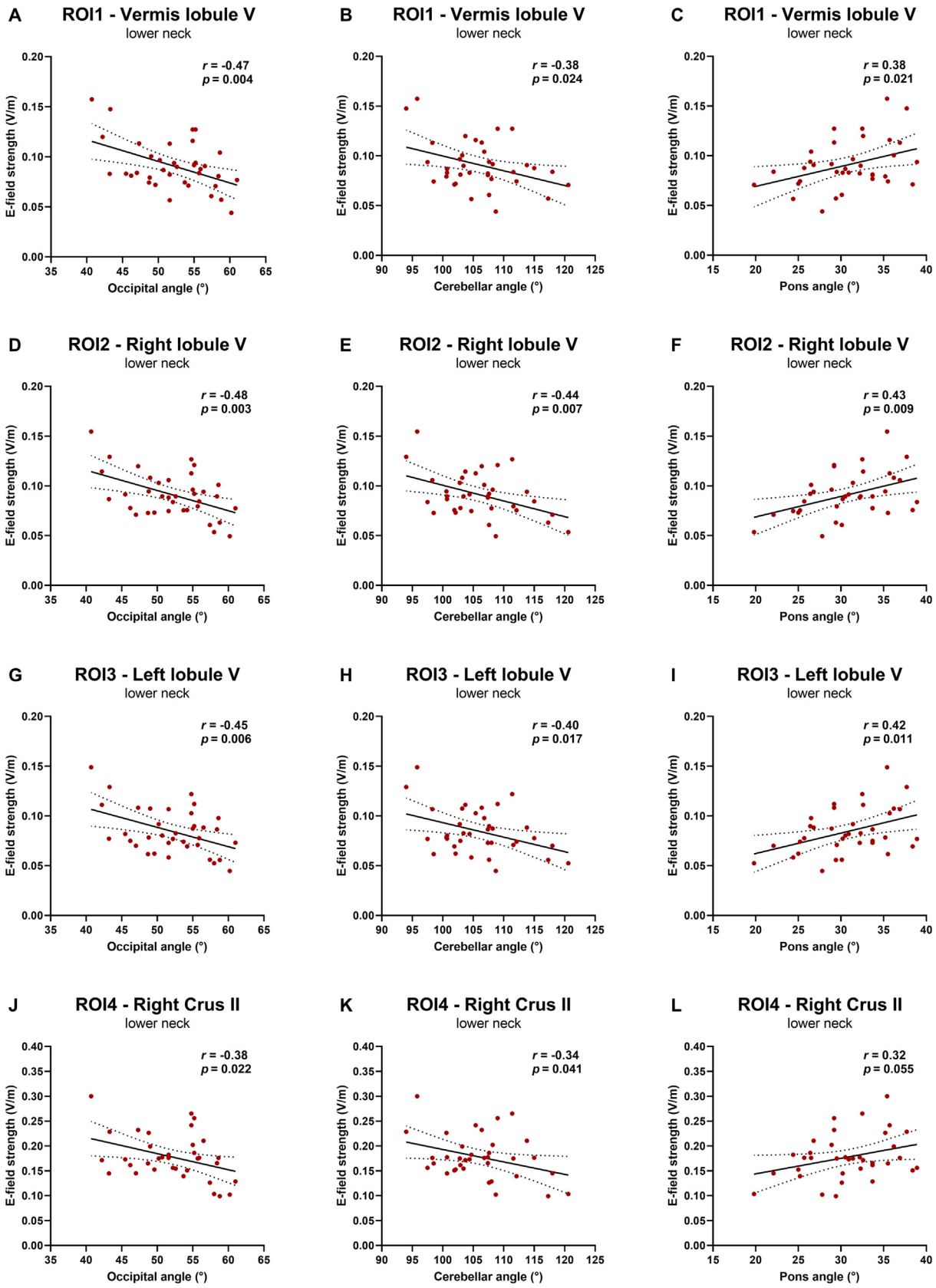

Fig. 8. Associations between electric field strengths in each of the eight selected regions of interest (ROIs) and occipital angle (A, D, G, J, M, P, S, and V), cerebellar angle (B, E, H, K, N, Q, T, and W), and pons angle (C, F, I, L, O, R, U, and X) using a lower neck montage.

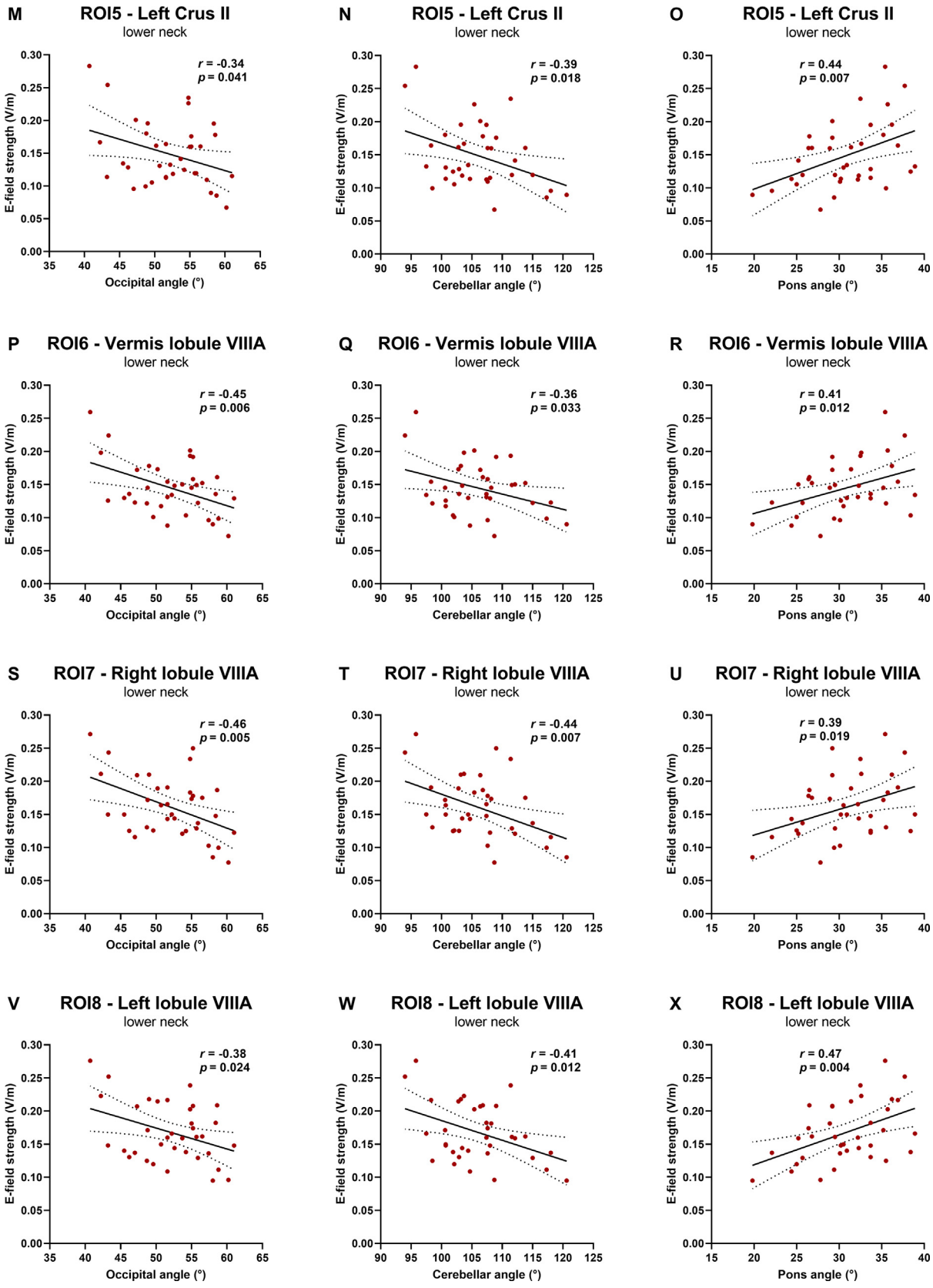

Fig. 8 (*continued*)

Table 1
Predictors of field strength induced by cerebellar transcranial direct current stimulation in five regions of interest (ROIs) using a lower neck montage. Skin-cerebellum distance (SCD), pons angle, cerebellar angle, and occipital angle were selected as independent variables.

	Predictors	R^2	ΔR^2	B	95% CI	Beta	P value
ROI1 – vermis lobule V	1. SCD	0.60	0.08	−0.003	−0.003; −0.002	−0.68	<0.001
	2. Pons angle			0.001	0.00; 0.003	0.29	0.014
ROI2 – right lobule V	1. SCD	0.69	0.10	−0.003	−0.004; −0.002	−0.72	<0.001
	2. Cerebellar angle			−0.001	−0.002; 0.00	−0.33	0.002
ROI4 – right Crus II	1. SCD	0.66	0.05	−0.007	−0.009; −0.005	−0.74	<0.001
	2. Cerebellar angle			−0.002	−0.003; 0.00	−0.23	0.033
ROI6 – vermis lobule VIIIA	1. SCD	0.64	0.09	−0.004	−0.006; −0.003	−0.70	<0.001
	2. Pons angle			0.003	0.001; 0.004	0.32	0.005
ROI7 – right lobule VIIIA	1. SCD	0.67	0.11	−0.006	−0.008; −0.005	−0.70	<0.001
	2. Cerebellar angle			−0.002	−0.004; −0.001	−0.33	0.002

B = unstandardized coefficient, beta = standardized coefficient, CI = confidence interval, ΔR^2 = change in R^2 compared with a model that only includes skin-cerebellum distance.

as a mega cisterna magna or a retrocerebellar arachnoid cyst, can be detected in this way. Notably, a mega cisterna magna was described as an incidental finding in 26 out of 833 healthy adolescents (3.1%) and identified as the most frequent structural brain anomaly (Sullivan et al., 2017). Although not extremely common, the unwitting inclusion of subjects with such anomalies in cerebellar tDCS studies may distort results, especially when sample sizes are small.

Based on our findings and those of others, there is a trade-off between focality and field strength in the target area when using conventional bipolar montages (Dmochowski et al., 2011). From a translational perspective, these observations may have the following implications. When focality is the primary goal (e.g., one rather specifically wants to modulate the excitability of neurons in lobule VII), an extracephalic reference electrode position may be preferred in combination with a higher current intensity. By contrast, in case of therapeutic purposes (e.g., to improve postural control in elderly people or in the treatment of patients with neuropsychiatric disorders), the main objective could be to obtain high electric field strengths within the cerebellum. In such a scenario, one might prefer a cephalic montage. However, it remains to be determined how increased spread of the current to extracerebellar regions, which was most prominent for the frontopolar montage, will affect clinical outcomes.

In conclusion, our results indicate that up to 70% of the variability in cerebellar tDCS-induced electric field strength can be explained by interindividual differences in skin-cerebellum distance and posterior fossa morphometry. Furthermore, when using a midline cerebellar tDCS approach, an extracephalic reference electrode was found to cause lower field strengths but higher field focality compared with cephalic montages. Additional work is required to establish clinical, behavioural, and neurophysiological correlates in healthy and disease states, which might eventually support individualized dosing of tDCS.

Funding

This study was funded by the National Ataxia Foundation and used data from ESMI, an EU Joint Programme – Neurodegenerative Disease Research (JPND) project (see https://www.jpnd.eu). ESMI is supported through the following funding organisations under the aegis of JPND: Germany, Federal Ministry of Education and Research (BMBF; funding codes 01ED1602A/B); Netherlands, The Netherlands Organisation for Health Research and Development; Portugal, Foundation for Science and Technology and Regional Fund for Science and Technology of the Azores; United Kingdom, Medical Research Council. ESMI has received funding from the European Union's Horizon 2020 research and innovation programme under grant agreement No 643417. At the US sites, ESMI was in part supported by the National Ataxia Foundation and the National Institute of Neurological Disorders and Stroke (NINDS) grant R01NS080816.

Declaration of interest

Roderick Maas receives research support from the National Ataxia Foundation. Jennifer Faber receives research support from the National Ataxia Foundation and as a fellow of the Hertie Network of Excellence in Clinical Neuroscience. Bart van de Warrenburg receives research support from ZonMw, NWO, Hersenstichting, Gossweiler Foundation, and Radboud university medical center, receives royalties from BSL – Springer Nature, and has served on a scientific advisory board of uniQure and Servier. Dennis Schutter receives research support from the Dutch Research Foundation (NWO, VI.C.181.005).

ESMI MR Study Group:

Thomas Klockgether receives or has received research support from the Deutsche Forschungsgemeinschaft (DFG), the Bundesministerium für Bildung und Forschung (BMBF), the Bundesministerium für Gesundheit (BMG), the Robert Bosch Foundation, the European Union (EU), and the National Institutes of Health (NIH). He has received consulting fees from Biohaven, uniQure, Vico Therapeutics, Roche, and UBC. He has received a speaker honorarium from Novartis and Bayer.

Gülin Öz receives research support from the National Institutes of Health and Biogen Inc., consults for IXICO Technologies Limited, serves on the Scientific Advisory Board of BrainSpec Inc, and has served on a clinical advisory board of uniQure.

Chiadi Onyike receives research support from the NIH, National Ataxia Foundation, the Robert and Nancy Hall Fund for Brain Research, and Alector. He is a consultant for Alector and Acadia.

Khalaf Bushara, Judith van Gaalen, Dagmar Timmann, Kathrin Reetz, and Heike Jacobi report no disclosures.

Appendix A

ESMI MR Study Group: Thomas Klockgether (Department of Neurology, University Hospital Bonn, and German Center for Neurodegenerative Diseases [DZNE], Bonn, Germany), Khalaf Bushara (Ataxia Center, Department of Neurology, University of Minnesota, Minneapolis, USA), Gülin Öz (Center for Magnetic Resonance Research, Department of Radiology, University of Minnesota, Minneapolis, USA), Judith van Gaalen (Department of Neurology, Donders Institute for Brain, Cognition, and Behaviour, Radboud University Medical Center, Nijmegen, the Netherlands), Dagmar Timmann (Department of Neurology and Center for Translational Neuro- and Behavioral Sciences [C-TNBS], Essen University Hospital, University of Duisburg-Essen, Essen, Germany), Kathrin Reetz (Department of Neurology, RWTH Aachen University, and JARA-BRAIN Institute Molecular Neuroscience and Neuroimaging,

Forschungszentrum Jülich GmbH and RWTH Aachen University, Aachen, Germany), Heike Jacobi (Department of Neurology, University Hospital Heidelberg, Heidelberg, Germany), Chiadi Onyike (Department of Psychiatry and Behavioral Sciences, Johns Hopkins University School of Medicine, Baltimore, USA).

Appendix B. Supplementary material

Supplementary data to this article can be found online at https://doi.org/10.1016/j.clinph.2023.06.019.

References

Antonenko D, Thielscher A, Saturnino GB, Aydin S, Ittermann B, Grittner U, et al. Towards precise brain stimulation: Is electric field simulation related to neuromodulation? Brain Stimul 2019;12(5):1159–68.

Azevedo FA, Carvalho LR, Grinberg LT, Farfel JM, Ferretti RE, Leite RE, et al. Equal numbers of neuronal and nonneuronal cells make the human brain an isometrically scaled-up primate brain. J Comp Neurol 2009;513(5):532–41.

Benussi A, Batsikadze G, Franca C, Cury RG, Maas RPPWM. The therapeutic potential of non-invasive and invasive cerebellar stimulation techniques in hereditary ataxias. Cells 2023;12(8):1193.

Benussi A, Dell'Era V, Cotelli MS, Turla M, Casali C, Padovani A, et al. Long term clinical and neurophysiological effects of cerebellar transcranial direct current stimulation in patients with neurodegenerative ataxia. Brain Stimul 2017;10(2):242–50.

Buckner RL, Krienen FM, Castellanos A, Diaz JC, Yeo BT. The organization of the human cerebellum estimated by intrinsic functional connectivity. J Neurophysiol 2011;106(5):2322–45.

Cattaneo Z, Ferrari C, Ciricugno A, Heleven E, Schutter D, Manto M, et al. New horizons on non-invasive brain stimulation of the social and affective cerebellum. Cerebellum 2022;21(3):482–96.

Craig CE, Doumas M. Anodal transcranial direct current stimulation shows minimal, measure-specific effects on dynamic postural control in young and older adults: A double blind, sham-controlled study. PLoS One 2017;12(1):e0170331.

Dmochowski JP, Datta A, Bikson M, Su Y, Parra LC. Optimized multi-electrode stimulation increases focality and intensity at target. J Neural Eng 2011;8(4):046011.

Ehsani F, Samaei A, Zoghi M, Hedayati R, Jaberzadeh S. The effects of cerebellar transcranial direct current stimulation on static and dynamic postural stability in older individuals: a randomized double-blind sham-controlled study. Eur J Neurosci 2017;46(12):2875–84.

Ferrucci R, Bocci T, Cortese F, Ruggiero F, Priori A. Cerebellar transcranial direct current stimulation in neurological disease. Cerebellum Ataxias 2016;3(1):16.

Ferrucci R, Giannicola G, Rosa M, Fumagalli M, Boggio PS, Hallett M, et al. Cerebellum and processing of negative facial emotions: cerebellar transcranial DC stimulation specifically enhances the emotional recognition of facial anger and sadness. Cogn Emot 2012;26(5):786–99.

Fertonani A, Miniussi C. Transcranial electrical stimulation: what we know and do not know about mechanisms. Neuroscientist 2017;23(2):109–23.

Gomez-Tames J, Asai A, Mikkonen M, Laakso I, Tanaka S, Uehara S, et al. Group-level and functional-region analysis of electric-field shape during cerebellar transcranial direct current stimulation with different electrode montages. J Neural Eng 2019;16(3):036001.

Grimaldi G, Argyropoulos GP, Bastian A, Cortes M, Davis NJ, Edwards DJ, et al. Cerebellar transcranial direct current stimulation (ctDCS): A novel approach to understanding cerebellar function in health and disease. Neuroscientist 2016;22(1):83–97.

Hulst T, John L, Kuper M, van der Geest JN, Goricke SL, Donchin O, et al. Cerebellar patients do not benefit from cerebellar or M1 transcranial direct current stimulation during force-field reaching adaptation. J Neurophysiol 2017;118(2):732–48.

Inukai Y, Saito K, Sasaki R, Kotan S, Nakagawa M, Onishi H. Influence of transcranial direct current stimulation to the cerebellum on standing posture control. Front Hum Neurosci 2016;10:325.

Jurcak V, Tsuzuki D, Dan I. 10/20, 10/10, and 10/5 systems revisited: their validity as relative head-surface-based positioning systems. Neuroimage 2007;34(4):1600–11.

King M, Hernandez-Castillo CR, Poldrack RA, Ivry RB, Diedrichsen J. Functional boundaries in the human cerebellum revealed by a multi-domain task battery. Nat Neurosci 2019;22(8):1371–8.

Klaus J, Schutter DJLG. Electrode montage-dependent intracranial variability in electric fields induced by cerebellar transcranial direct current stimulation. Sci Rep 2021;11(1):22183.

Krienen FM, Buckner RL. Segregated fronto-cerebellar circuits revealed by intrinsic functional connectivity. Cereb Cortex 2009;19(10):2485–97.

Laakso I, Mikkonen M, Koyama S, Hirata A, Tanaka S. Can electric fields explain inter-individual variability in transcranial direct current stimulation of the motor cortex? Sci Rep 2019;9(1):626.

Li LM, Uehara K, Hanakawa T. The contribution of interindividual factors to variability of response in transcranial direct current stimulation studies. Front Cell Neurosci 2015;9:181.

Luft AR, Skalej M, Schulz JB, Welte D, Kolb R, Burk K, et al. Patterns of age-related shrinkage in cerebellum and brainstem observed in vivo using three-dimensional MRI volumetry. Cereb Cortex 1999;9(7):712–21.

Maas RPPWM, Helmich RCG, van de Warrenburg BPC. The role of the cerebellum in degenerative ataxias and essential tremor: Insights from noninvasive modulation of cerebellar activity. Mov Disord 2020;35(2):215–27.

Maas RPPWM, Schutter DJLG, Toni I, Timmann D, van de Warrenburg BPC. Cerebellar transcranial direct current stimulation modulates timing but not acquisition of conditioned eyeblink responses in SCA3 patients. Brain Stimul 2022a;15(3):806–13.

Maas RPPWM, Teerenstra S, Toni I, Klockgether T, Schutter D, van de Warrenburg BPC. Cerebellar transcranial direct current stimulation in spinocerebellar ataxia type 3: a randomized, double-blind, sham-controlled trial. Neurotherapeutics 2022b;19(4):1259–72.

Manto M, Argyropoulos GPD, Bocci T, Celnik PA, Corben LA, Guidetti M, et al. Consensus paper: novel directions and next steps of non-invasive brain stimulation of the cerebellum in health and disease. Cerebellum 2022;21(6):1092–122.

Mosayebi-Samani M, Jamil A, Salvador R, Ruffini G, Haueisen J, Nitsche MA. The impact of individual electrical fields and anatomical factors on the neurophysiological outcomes of tDCS: A TMS-MEP and MRI study. Brain Stimul 2021;14(2):316–26.

Nandi T, Puonti O, Clarke WT, Nettekoven C, Barron HC, Kolasinski J, et al. tDCS induced GABA change is associated with the simulated electric field in M1, an effect mediated by grey matter volume in the MRS voxel. Brain Stimul 2022;15(5):1153–62.

Oldrati V, Schutter DJLG. Targeting the human cerebellum with transcranial direct current stimulation to modulate behavior: a meta-analysis. Cerebellum 2018;17(2):228–36.

Opitz A, Paulus W, Will S, Antunes A, Thielscher A. Determinants of the electric field during transcranial direct current stimulation. Neuroimage 2015;109:140–50.

Panouilleres MT, Miall RC, Jenkinson N. The role of the posterior cerebellum in saccadic adaptation: a transcranial direct current stimulation study. J Neurosci 2015;35(14):5471–9.

Parazzini M, Rossi E, Ferrucci R, Liorni I, Priori A, Ravazzani P. Modelling the electric field and the current density generated by cerebellar transcranial DC stimulation in humans. Clin Neurophysiol 2014;125(3):577–84.

Polania R, Nitsche MA, Ruff CC. Studying and modifying brain function with non-invasive brain stimulation. Nat Neurosci 2018;21(2):174–87.

Rampersad SM, Janssen AM, Lucka F, Aydin U, Lanfer B, Lew S, et al. Simulating transcranial direct current stimulation with a detailed anisotropic human head model. IEEE Trans Neural Syst Rehabil Eng 2014;22(3):441–52.

Rezaee Z, Dutta A. Cerebellar lobules optimal stimulation (CLOS): A computational pipeline to optimize cerebellar lobule-specific electric field distribution. Front Neurosci 2019;13:266.

Rezaee Z, Dutta A. Lobule-specific dosage considerations for cerebellar transcranial direct current stimulation during healthy aging: A computational modeling study using age-specific magnetic resonance imaging templates. Neuromodulation 2020;23(3):341–65.

Saturnino GB, Puonti O, Nielsen JD, Antonenko D, Madsen KH, Thielscher A. SimNIBS 2.1: A Comprehensive Pipeline for Individualized Electric Field Modelling for Transcranial Brain Stimulation. In: Makarov S, Horner M, Noetscher G, editors. Brain and Human Body Modeling: Computational Human Modeling at EMBC 2018. Cham (CH); 2019. p. 3–25.

Schmahmann JD. The cerebellum and cognition. Neurosci Lett 2019;688:62–75.

Schmitz-Hubsch T, Tezenas du Montcel S, Baliko L, Berciano J, Boesch S, Depondt C, et al. Scale for the assessment and rating of ataxia: development of a new clinical scale. Neurology 2006;66(11):1717–20.

Sereno MI, Diedrichsen J, Tachrount M, Testa-Silva G, d'Arceuil H, De Zeeuw C. The human cerebellum has almost 80% of the surface area of the neocortex. Proc Natl Acad Sci U S A 2020;117(32):19538–43.

Steiner KM, Enders A, Thier W, Batsikadze G, Ludolph N, Ilg W, et al. Cerebellar tDCS Does Not Improve Learning in a Complex Whole Body Dynamic Balance Task in Young Healthy Subjects. PLoS One 2016;11(9):e0163598.

Stoodley CJ, Schmahmann JD. Evidence for topographic organization in the cerebellum of motor control versus cognitive and affective processing. Cortex 2010;46(7):831–44.

Sullivan EV, Lane B, Kwon D, Meloy MJ, Tapert SF, Brown SA, et al. Structural brain anomalies in healthy adolescents in the NCANDA cohort: relation to neuropsychological test performance, sex, and ethnicity. Brain Imaging Behav 2017;11(5):1302–15.

van Dun K, Bodranghien FC, Marien P, Manto MU. tDCS of the cerebellum: where do we stand in 2016? Technical issues and critical review of the literature. Front Hum Neurosci 2016;10:199.

Wagner TA, Zahn M, Grodzinsky AJ, Pascual-Leone A. Three-dimensional head model simulation of transcranial magnetic stimulation. IEEE Trans Biomed Eng 2004;51(9):1586–98.

Windhoff M, Opitz A, Thielscher A. Electric field calculations in brain stimulation based on finite elements: an optimized processing pipeline for the generation and usage of accurate individual head models. Hum Brain Mapp 2013;34(4):923–35.

Yushkevich PA, Piven J, Hazlett HC, Smith RG, Ho S, Gee JC, et al. User-guided 3D active contour segmentation of anatomical structures: significantly improved efficiency and reliability. Neuroimage 2006;31(3):1116–28.